



Broadband graphene and metasurface-loaded solar thermal absorber design for visible and infrared regions

W. Rajan Babu¹ · P. Rathina Kumar² · L. Murali³ · N. K. Anushkannan⁴

Received: 16 July 2022 / Accepted: 26 October 2022 / Published online: 12 December 2022
© The Author(s), under exclusive licence to Springer Science+Business Media, LLC, part of Springer Nature 2022

Abstract

Solar energy is a renewable energy source that can meet high energy demands without affecting mother earth. We have proposed a solar absorber design that has high absorption results for visible and infrared regions. Two different sizes metasurface resonator design is observed to find the best design for the solar absorber. The metasurface design with higher length and width is showing better absorption for visible and infrared regions. The metasurface design 1 is giving 90% average absorption and 97% highest absorption in the visible region and 88% average absorption in the infrared range of 0.7–1.5 μm . The optimized parameters are obtained for substrate variations like its thickness, length and width. The variation of thickness of resonating element is also carried out. The angle of incidence is showing good absorption for the range of 0–20° and 40–70°. The electric field intensity results are presented in V/m with red color high values and blue color low values.

Keywords Absorber · Broadband · Graphene · Infrared · Metasurface · Solar · Visible

1 Introduction

Solar absorbers are absorbing solar energy and convert it to thermal energy which can be used for different applications of heating, etc. (Wan et al. 2015; Muhammad et al. 2019). The efficiency of these solar absorbers is very important as the rise in efficiency will make them more affordable and efficient in renewable and sustainable energy generation (Patel et al. 2022a). The material of the solar absorber plays a vital role in its

✉ W. Rajan Babu
rajanbabu.w@sece.ac.in

¹ Department of Electrical and Electronics Engineering, Sri Eshwar College of Engineering, Coimbatore, Tamilnadu 641202, India

² Department of Electronics and Communication Engineering, College of Engineering and Technology, SRM Institute of Science and Technology, Vadapalani Campus, Chennai, Tamilnadu 600026, India

³ Department of Electronics and Communication Engineering, P. A. College of Engineering and Technology, Pollachi, Tamilnadu 642002, India

⁴ Department of Electronics and Communication Engineering, Kathir College of Engineering, Coimbatore, Tamilnadu 641062, India

absorption. Many researchers all over the world are working on different materials to improve the absorption of the solar absorber (Sekhi et al. 2020; Baqir et al. 2021; Te et al. 2020). The solar absorber efficiency can be improved by incorporating graphene and loading metasurface in them (Cen et al. 2019; Mahmud et al. 2021; Surve et al. 2021). In the following, we are reviewing the literature based on graphene solar absorbers and metasurface solar absorbers.

Metamaterials is introduced by vasselago theoretically in 1968 (Veselago 1968) and practically proved by smith and his team later (Smith et al. 2000). Metamaterials are artificial materials that can be introduced into natural materials to improve their capacity and properties (Patel et al. 2020a). The split-ring resonator and thin wires are the two components that introduced the negative behavior in metamaterials (Patel and Parmar 2021). Metamaterials are used in several applications like sensing, absorbing, antennas, etc. (Shen and Xiong 2022; Vafapour et al. 2021; Nguyen et al. 2022; Ahmadivand et al. 2021). One of the effective applications is in designing solar absorbers. These metamaterial components are introduced in solar absorbers to improve their efficiency and reduce their cost. Broadband behavior can be achieved using a metamaterial absorber made with germanium-based resonating structures (Guo et al. 2022). Solar thermal absorbers are created using metamaterial loading which is applicable in heating applications (Li et al. 2021). Broadband metamaterial-based solar absorber design with absorptivity of about 80% is achieved in triple-layer thin-film design (Hoque and Islam 2020). A metamaterial absorber with swastika-shaped is achieved. The absorption level is increased by the swastika-shaped design and broadband results are achieved. The polarization independent ness is also achieved (Patel et al. 2022b). The metamaterial-based solar absorber is designed with different material disks. The broadband and polarization-independent behavior are achieved using these structures (Liang et al. 2019) Gold material-based metamaterial resonators are used to achieve broadband infrared absorbers. The array of gold disks is used to obtain this response (Patel et al. 2020b).

Graphene is a single-atom-thick graphite material that can be used in solar absorbers because of its extensive electrical and optical properties. Its usage can increase solar absorber's absorption. The graphene layer can be used as a spacer for this improvement. Graphene-based solar absorbers can be used to achieve broadband, polarization-independent, and wide-angle solar absorbers. Graphene oxide is a material that can be incorporated with metamaterials which improve broadband absorption (Saurabh et al. 2022). Plus-shaped metasurface based on graphene material creates a resonating structure that absorbs broadband absorption which results in a broadband absorber (Patel et al. 2019). The design is giving 70% absorption in the solar region (Rufangura and Sabah 2017). The pyramid-shaped metamaterial absorber based on graphene can get an absorption of around 89% in the visible region (Charola et al. 2020). About 90% efficient solar to thermal absorber is designed with the use of graphene metamaterial array structure placed over the substrate (Patel et al. 2021a; Jadeja et al. 2020; Lin et al. 2019). The solar absorber can be used for many applications and some of the applications are solar thermal heating, solar cells, heat transfer systems, and optoelectronic devices (Klug et al. 2020; Bilal et al. 2020; Ogawa and Kimata 2018; Zhang et al. 2020).

The solar absorber design needs to be efficient to be applicable in solar thermal energy applications. The solar absorber design needs to be absorbing visible, infrared, and ultraviolet energies to be efficiently applicable in major solar applications. We proposed a graphene-based metamaterial design that gives a broadband absorption region which covers the visible and infrared regions with nearly more than 90% average absorption. The design results are also investigated for electric field and variation

in different parameters. The following sections present the solar absorber design and its results.

2 Metasurface designs

The metasurface design is created by placing a line between three parallel lines as presented in Fig. 1. The metasurface design is created with the gap between the lines producing capacitance and the lines producing inductance and thus the resonance is affected by the metasurface design. Two different metasurface designs are created by reducing the size of resonator as shown in Fig. 1. The metasurface design is made up of Titanium material and it is placed over SiO_2 material. The titanium material is used as resonator as it is a low-cost material compared to gold and silver metals. The graphene layer is sandwiched between the titanium and SiO_2 layers. A single layer of graphene material is used having a thickness 0.34 nm. The two metasurface design and their shapes are presented in Fig. 1. The Metasurface 1 design is having a length (L_2) of 3000 nm and width (W_1) of 600 nm. The Metasurface 2 design is having a length (L_3) of 2000 nm and width (W_2) of 400 nm. The results of metasurface designs discussed later.

Absorption analysis is presented in Patel et al. 2021b and equations are presented below.

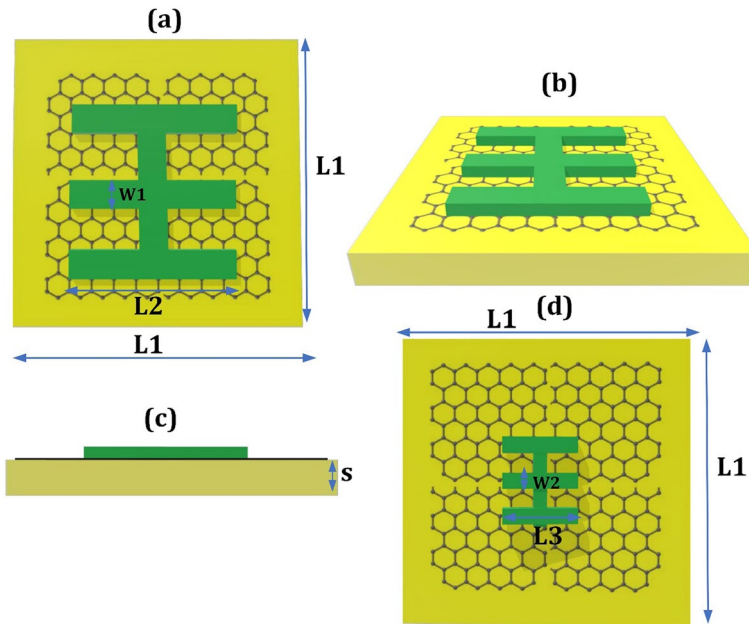


Fig. 1 Metasurface design with two different sizes for solar absorber **a** metasurface Resonator 1 design with W_1 and L_2 , **b** 3D view of Resonator 1 design (2) Front view of Resonator 1 design **b** Metasurface Resonator two design with W_2 and L_3 . The different parameters are $L_1=6000$ nm, $L_2=3000$ nm, $W_1=600$ nm, $L_3=2000$ nm, $W_2=400$ nm, $S=2500$ nm. The graphene layer is 0.34 nm thick. The figure is not upto the scale

$$r(\omega, \theta_i) = \frac{\omega \cos \theta_i \prod_{00}(\omega, \theta_i)}{2i\hbar ck^2 + \omega \cos \theta_i \prod_{00}(\omega, \theta_i)} \quad (1)$$

$$\sigma_{||}(\omega, k) = -i \frac{\omega}{4\pi\hbar k^2} \prod_{00}(\omega, k) \quad (2)$$

$$r(\omega, \theta_i) = \frac{2\pi \cos \theta_i \sigma_{||}(\omega, k)}{c + 2\pi \cos \theta_i \sigma_{||}(\omega, k)} \quad (3)$$

$$\mathcal{R}(\omega, \theta_i) = |r(\omega, \theta_i)|^2 \quad (4)$$

$$\mathcal{R}(\omega, \theta_i) = \frac{4\pi^2 \cos^2 \theta_i [\operatorname{Re}^2 \sigma_{||}(\omega, k) + \operatorname{Im}^2 \sigma_{||}(\omega, k)]}{[c + 2\pi \cos \theta_i \operatorname{Re} \sigma_{||}(\omega, k)]^2 + 4\pi^2 \cos^2 \theta_i \operatorname{Im}^2 \sigma_{||}(\omega, k)} \quad (5)$$

$$\mathcal{R}(\omega) = \mathcal{R}(\omega, 0) = \frac{4\pi^2 [\operatorname{Re}^2 \sigma(\omega) + \operatorname{Im}^2 \sigma(\omega)]}{[c + 2\pi \operatorname{Re} \sigma(\omega)]^2 + 4\pi^2 \operatorname{Im}^2 \sigma(\omega)} \quad (6)$$

$$A(\omega) = 1 - \mathcal{R}(\omega) - T(\omega) \quad (7)$$

where k refers to the wave vector.

The graphene chemical potential and its effect are presented in Patel et al. 2022c and equations are presented below.

$$\varepsilon(\omega) = 1 + \frac{\sigma_s}{\varepsilon_0 \omega \Delta} \quad (8)$$

$$\sigma_{intra} = \frac{-je^2 k_B T}{\pi \hbar^2 (\omega - j2\Gamma)} \left(\frac{\mu_c}{k_B T} + 2 \ln \left(e^{-\frac{\mu_c}{k_B T}} + 1 \right) \right) \quad (9)$$

$$\sigma_{inter} = \frac{-je^2}{4\pi \hbar} \ln \left(\frac{2|\mu_c| - (\omega - j2\Gamma)\hbar}{2|\mu_c| + (\omega - j2\Gamma)\hbar} \right) \quad (10)$$

$$\sigma_s = \sigma_{inter} + \sigma_{intra} \quad (11)$$

3 Results and discussions

The two metasurface designs made up of changing their length and width are simulated using COMSOL Multiphysics. The simulator is used effectively to achieve the broadband absorption and results are presented. The results for the two designs are compared in Fig. 2. The metasurface 1 design (with higher length and width)'s result is presented in Fig. 2a which shows that the absorption is high for the whole wavelength range while the

Fig. 2 Absorption result for visible and infrared regions **a** metasurface design 1 with high length and width **b** metasurface design 2 with low length and width. The metasurface 1 design having higher length and width is giving better performance. The 90% for metasurface design 1 with the highest peak absorption of 97% for 0.75 μm . The metasurface design 2 with 63% with a peak absorption of 97.6% at 0.44 μm

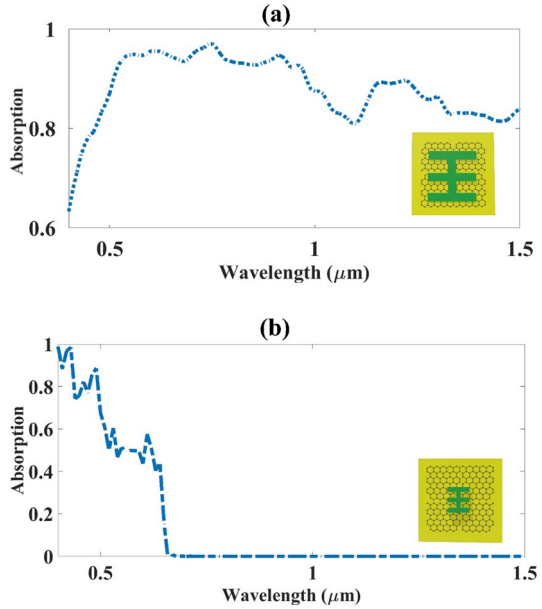


Table 1 Two metasurface design comparison

Design	0.4–0.7 μm absorption (%)	0.7–1.5 μm absorption (%)
Metasurface design 1	90	88
Metasurface design 2	63	–

metasurface 2 design (with lower length and width)’s absorption is reducing as it moves ahead from 0.67 μm and reduces to almost zero. The average absorption for both designs is compared in Table 1 for visible and infrared regions. The average absorption of design 1 is 90% in the visible region compared to 63% of design 2. Design 1 has an 88% average absorption in the infrared range of 0.7–1.5 μm . The highest absorption peaks of 97% and 97.6% are achieved for design-1 and design-2 respectively.

3.1 Optimization

Parametric optimization is very important in designing any solar absorber so that the best and most efficient solar absorber can be designed (Patel et al. 2020c). The parametric optimization can be performed for different substrate and metasurface parameters. The optimization can also be performed for an angle of incidence and graphene chemical potential. We have used all these optimizations to get the optimized design. In the series of these optimizations, the first is metasurface thickness optimization. Optimized values are obtained by varying the metasurface thickness from 1000 to 2000 nm. The wavelength is varied between 0.4 and 1.5 μm . The initial value of metasurface thickness gives the absorption of the solar absorber having good values throughout the spectrum observed. As soon as the metasurface thickness is increased the inductance of the overall structure

is increasing which is affecting the absorption of the design. The increase in metasurface thickness gives good absorption in the initially visible region but in an infrared region, the absorption is decreasing. The decrease in absorption for the infrared region is visible for the highest metasurface thickness of 2000 nm. The green color dot marker curve clearly shows this observation. The response of 1750 nm thickness is also very similar to 2000 nm and for the infrared region, the absorption is very less. So from the observation, it is clear that the overall absorption is good for 1000 nm metasurface thickness. For all the other variations the absorption is changing in different regions, but the overall absorption is similar to or less than the 1000 nm metasurface thickness.

The second optimization observed is for Substrate thickness. Optimized values are obtained by varying the substrate thickness from 2500 to 3500 nm. The wavelength is varied between 0.4 and 1.5 μm . The initial value of substrate thickness gives the absorption of the solar absorber having good values throughout the spectrum observed. As soon as the substrate thickness is increased, the absorption of the visible region is not affected much but for the infrared region absorption drastically decreases. The decrease in absorption for the infrared region is visible for the highest substrate thickness 3500 nm. The middle thickness of 3000 nm has good absorption in visible and good absorption in half infrared range

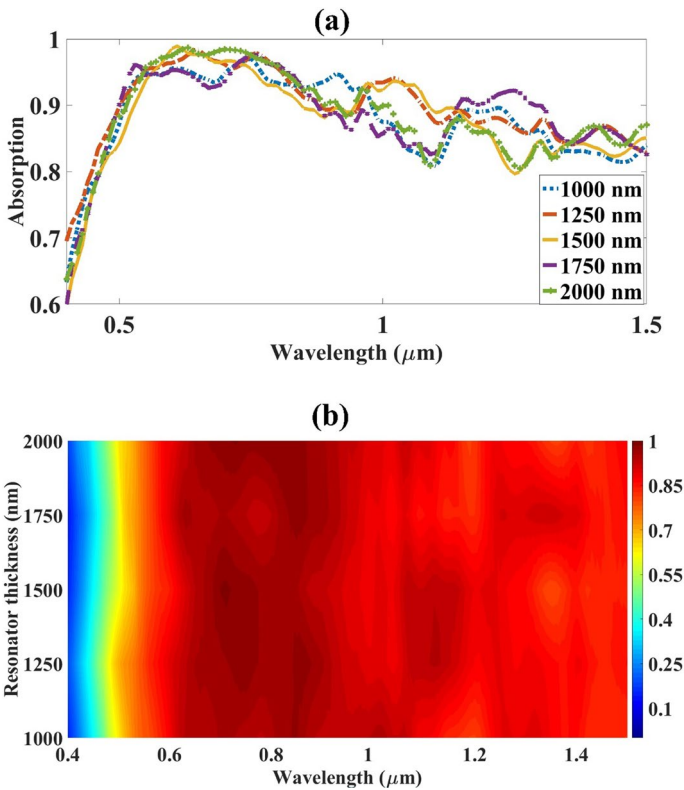


Fig. 3 Optimization of resonator thickness. **a** Line plot, **b** color plot. The thickness varied from 1000 to 2000 nm. The absorption for the initial thickness of 1000 nm has good absorption for the whole range and or higher thickness of 2000 nm has good absorption in visible while less absorption in the infrared range. The optimized value of resonator thickness is 1000 nm

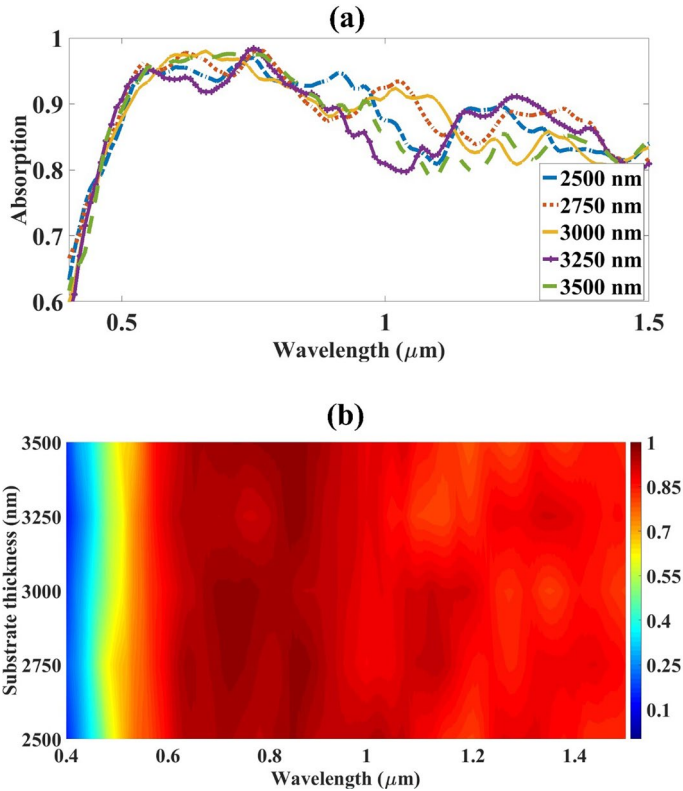


Fig. 4 Optimization of substrate thickness. **a** Line plot, **b** color plot. The thickness varied from 1000 to 2000 nm. The absorption for the initial thickness of 2500 nm has good absorption for the whole range and or higher thickness of 3500 nm has average absorption in visible while less absorption in the infrared range. The optimized value of resonator thickness is 1000 nm

till 1 μm but above this wavelength, the absorption is decreasing drastically. So from the observation, it is clear that the overall absorption is good for 2500 nm substrate thickness. For all the other variations the absorption is changing in different regions, but the overall absorption is similar to or less than the 2500 nm substrate thickness (Figs. 3, 4, 5, and 6).

The third optimization observed is for Substrate length. Optimized values are obtained by varying the substrate length from 6000 to 9000 nm. The wavelength is varied between 0.4 and 1.5 μm . The initial value of substrate length of 6000 nm and 7000 nm gives the absorption for the visible region but it is decreasing in the infrared region for 7000 nm length. The length is further increased to 8000 nm which shifts the absorption spectrum to 0.1 μm and the absorption is decreasing in the infrared region. The 9000 nm length further shifts the spectrum to 0.1 μm . The tuning in the absorption spectrum is visible for the higher length of the substrate. So from the observation, it is clear that the overall absorption is good for 6000 nm substrate length. For all the other variations the absorption is changing in different regions, but the overall absorption is higher for 6000 nm substrate length.

The fourth optimization observed is for Substrate width. Optimized values are obtained by varying the substrate width from 6000 to 9000 nm. The wavelength is varied between

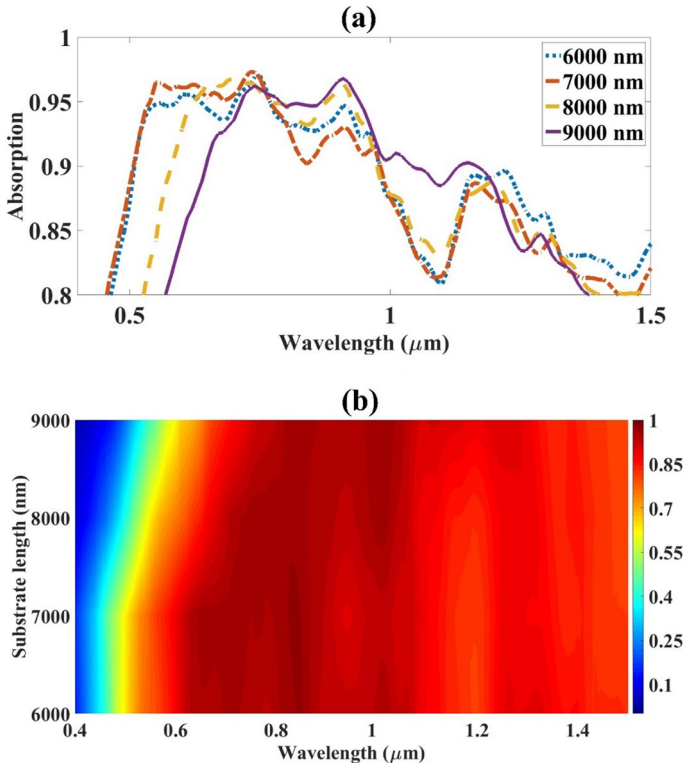


Fig. 5 Optimization of substrate length. **a** Line plot, **b** color plot. The length varied from 6000 to 9000 nm. The absorption for the initial length of 6000 nm and 7000 nm has good absorption for the whole visible range but it is decreasing in the infrared region for 7000 nm. For the 8000 nm and 9000 nm, the tuning in wavelength is achieved as absorption is shifted in the visible region. The optimized value of substrate length is 6000 nm

0.4 and 1.5 μm . The initial value of substrate width of 6000 nm is less initially in the visible region compared to 7000 nm width. For the rest of the wavelength range, the 6000 nm has higher absorption compared to the 7000 nm range. The length is further increased to 8000 nm which shifts the absorption spectrum to 0.1 μm and the absorption is decreasing in the infrared region. The 9000 nm length further shifts the spectrum to 0.1 μm . The tuning in the absorption spectrum is visible for the higher length of the substrate. So from the observation, it is clear that the overall absorption is good for 6000 nm substrate length. For all the other variations the absorption is changing in different regions, but the overall absorption is higher for 6000 nm substrate length.

3.2 Angle variation and graphene variation

Angle variation changes the light variation and the light intensity changes during the day so it is very important. The variation in angle is observed in Fig. 7a. The angle variation clearly shows that for angles 30° and 80° . The absorption is minimum which is visible with blue color in the plot. All other angles on incidences show good absorption for the whole wavelength

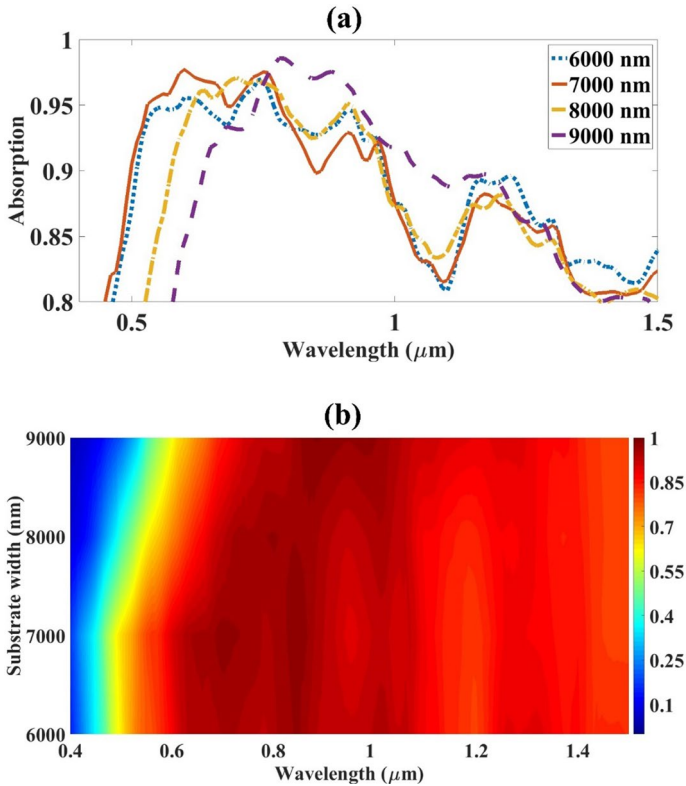


Fig. 6 Optimization of substrate width. **a** Line plot, **b** color plot. The width varied from 6000 to 9000 nm. The absorption for the initial width of 6000 nm is less initially in the visible region compared to the 7000 nm width. Overall, the absorption is good for 6000 nm width. The wavelength tuning is visible for 8000 nm and 9000 nm widths

range. The initial wavelength of 0.4 μm is having minimum absorption but it increases immediately as it is increased. For the angle, 60° and 70° has good values. The variation of graphene chemical potential and its effect on is presented in Fig. 7b. The variation results clearly show that there is no variation in absorption results for different variations in graphene chemical potential. The graphene potential variation is not affecting the absorption spectrum because of its observed wavelength range (Fig. 8).

3.3 Electric field Intensity (EFI)

The EFI of the metasurface absorber is investigated with four different wavelengths of the visible region. To observe the effect of the electric field in the major part of the visible region, four wavelengths are selected. The wavelengths 0.4 to 0.7 μm are investigated with a 0.1 μm step size. The absorption is minimum for 0.4 μm and maximum for 0.6 μm which is also

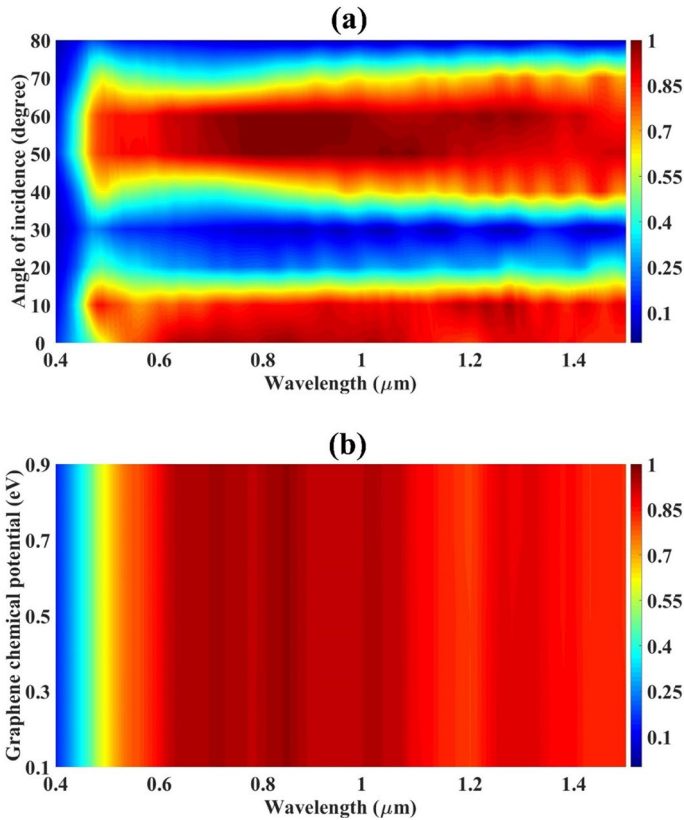


Fig. 7 Absorption results of metasurface 1 design for different values of **a** angle of incidence **b** graphene chemical potential. There is no variation in absorption results for the variation of graphene chemical potential for 0.1–0.9 eV. The angle of incidence is showing good absorption for 0–20° and 40–70°

similar to the absorption response achieved. The comparison of the proposed design is done with other designs in Table 2.

4 Conclusion

We have designed two metasurface-based solar absorbers using graphene material. The two designs are having different sizes with a similar shapes. Both designs are investigated to observe the solar absorber's absorption response in the wavelength range of 0.4–1.5 μm . The visible region and infrared regions are investigated in these proposed design results. The metasurface design 1 is giving 90% average absorption and 97% highest absorption in the visible region and 88% average absorption in the infrared range of 0.7–1.5 μm . The design results of metasurface design-1 are optimized for better absorption. The optimized parameter obtained for different parameters is substrate thickness of 2500 nm, substrate length and width of 6000 nm each, and resonator thickness of 1000 nm. The absorber is also showing the wide-angle of incidence covering

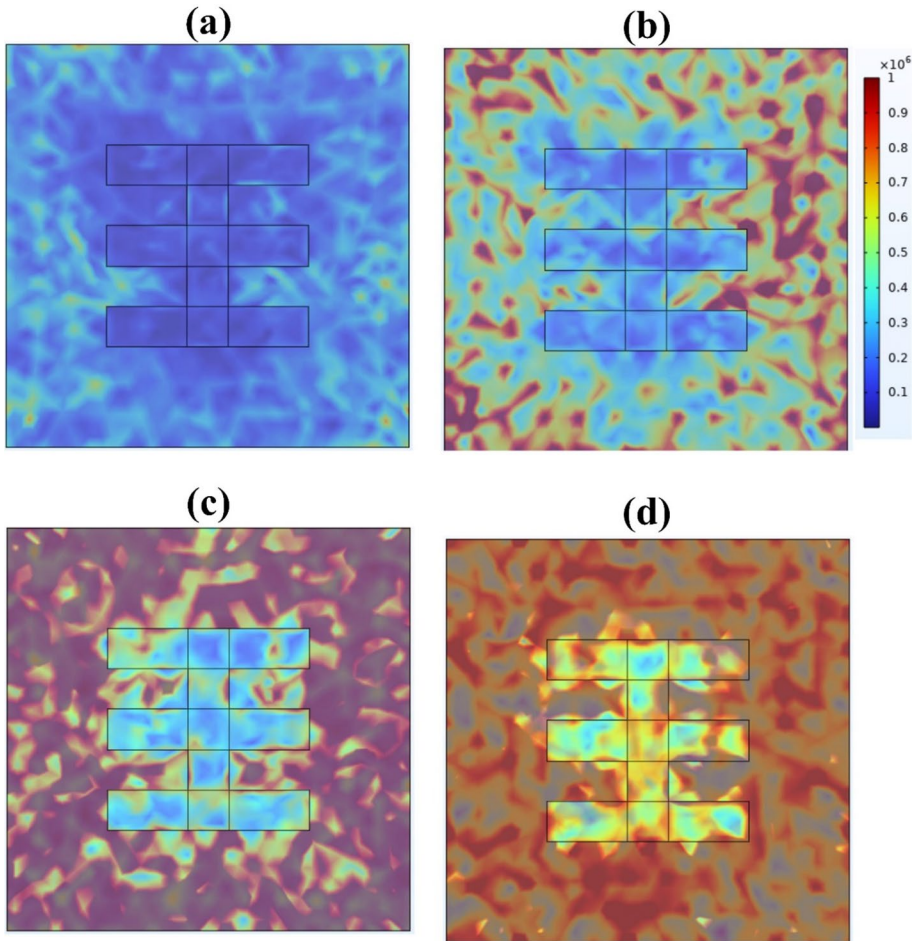


Fig. 8 Electric field intensity in V/m. **a** 0.4 μm , **b** 0.5 μm , **c** 0.6 μm , and **d** 0.7 μm . The minimum absorption is at 0.4

Table 2 Comparison of the proposed designs with similar published designs from reference

Design	0.4–0.7 μm absorption (%)	0.7–1.5 μm absorption (%)
Metasurface design 1	90	88
Metasurface design 2	63	–
From Rufangura and Sabah (2017)	70	–
From Musa et al. (2022)	80	80
From Azad et al. (2016)	90	–
From Patel et al. (2020d)	86.5	–
From Liu et al. (2018)	80	–
From Sang et al. (2019)	71.1	–
From Yu et al. (2019)	90	–
From Cao and Cheng (2019)	90	–

the whole range except 30° and 80° . The graphene's potential effect is not visible in observed wavelength region. The proposed solar absorber has the potential to be used in solar thermal energy conversion devices.

Author contributions All authors contributed to the study conception and design. WRB and PRK have done the numerical analysis for the article. LM and NKAK have experienced the results with proper fabrication and optimization. WRB has validated the complete work and prepared the first draft of the manuscript. All authors commented on previous versions of the manuscript. All authors read and approved the final manuscript.

Funding No funding is received for this research.

Availability of data and materials The data and materials used in this research will be made available at a reasonable request to the corresponding author.

Declarations

Conflict of interest The authors declared that there is no conflict of interest.

Ethical approval This declaration is "not applicable".

References

- Ahmadivand, A., Gerislioglu, B., Ramezani, Z., Kaushik, A., Manickam, P., Ghoreishi, S.A.: Functionalized terahertz plasmonic metasensors: femtomolar-level detection of SARS-CoV-2 spike proteins. *Biosens. Bioelectron.* **177**, 112971 (2021)
- Azad, A.K., Kort-Kamp, W.J.M., Sykora, M., et al.: Metasurface broadband solar absorber. *Sci. Rep.* **6**, 1–6 (2016)
- Baqir, M.A., Choudhury, P.K., Akhtar, M.N.: ZrN fractal-graphene-based metamaterial absorber in the visible and near-IR regimes. *Optik (stuttg.)* **237**, 166769 (2021)
- Bilal, R.M.H., Baqir, M.A., Choudhury, P.K., Naveed, M.A., Ali, M.M., Rahim, A.A.: Ultrathin broadband metasurface-based absorber comprised of tungsten nanowires. *Results Phys.* **19**, 103471 (2020)
- Cao, C., Cheng, Y.: A broadband plasmonic light absorber based on a tungsten meander-ring-resonator in visible region. *Appl. Phys. A Mater. Sci. Process.* **125**(1), 1–8 (2019)
- Cen, C., et al.: Theoretical design of a triple-band perfect metamaterial absorber in the THz frequency range. *Res. Phys.* **14**, 102463 (2019)
- Charola, S., Patel, S.K., Parmar, J., Ladumor, M., Dhasarathan, V.: Broadband graphene-based metasurface solar absorber. *Microw. Opt. Technol. Lett.* **62**(3), 1366–1373 (2020)
- Guo, K.L., Chen, H.H., Huang, X.M., Hu, T.H., Liu, H.Y.: Solar broadband metamaterial perfect absorber based on dielectric resonant structure of Ge cone array and InAs film. *Chin. Phys. B* **30**, 114201 (2022)
- Hoque, A., Islam, M.T.: Numerical analysis of single negative broadband metamaterial absorber based on tri thin layer material in visible spectrum for solar cell energy harvesting. *Plasmonics* **15**, 1061–1069 (2020)
- Jadeja, R., Charola, S., Patel, S.K., et al.: Numerical investigation of graphene-based efficient and broadband metasurface for terahertz solar absorber. *J. Mater. Sci.* **55**(8), 3462–3469 (2020)
- Klug, M.T., Milot, R.L., Milot, R.L., et al.: Metal composition influences optoelectronic quality in mixed-metal lead-tin triiodide perovskite solar absorbers. *Energy Environ. Sci.* **13**, 1776–1787 (2020)
- Li, Y., Lin, C., Wu, Z., et al.: Solution-processed all-ceramic plasmonic metamaterials for efficient solar-thermal conversion over $100\text{--}727^\circ\text{C}$. *Adv. Mater.* **33**, 2005074 (2021)
- Liang, C., Zhang, Y., Yi, Z., et al.: A broadband and polarization-independent metamaterial perfect absorber with monolayer Cr and Ti elliptical disks array. *Results Phys.* **15**, 102635 (2019)
- Lin, H., Sturmberg, B.C.P., Lin, K.T., et al.: A 90-nm-thick graphene metamaterial for strong and extremely broadband absorption of unpolarized light. *Nat. Photonics* **13**, 270–276 (2019)

- Liu, B., Tang, C., Chen, J., et al.: Multiband and broadband absorption enhancement of monolayer graphene at optical frequencies from multiple magnetic dipole resonances in metamaterials. *Nanoscale Res. Lett.* **13**, 1–7 (2018)
- Mahmud, S., Karim, M., Islam, S.S., et al.: A multi-band near perfect polarization and angular insensitive metamaterial absorber with a simple octagonal resonator for visible wavelength. *IEEE Access* **9**, 117746–117760 (2021)
- Muhammad, N., Tang, X., Tao, F., Qiang, L., Zhengbiao, O.: Broadband polarization-insensitive absorption by metasurface with metallic pieces for energy harvesting application. *Mater. Sci. Eng. B Solid-State Mater. Adv. Technol.* **249**, 114419 (2019)
- Musa, A., Hakim, M.L., Alam, T., et al.: Polarization independent metamaterial absorber with anti-reflection coating nanoarchitectonics for visible and infrared window applications. *Materials (basel)* **15**(10), 3733 (2022)
- Nguyen TK, Patel SK, Lavadiya S, Parmar J, Bui CD (2022) Design and fabrication of multiband reconfigurable copper and liquid multiple complementary split-ring resonator based patch antenna. *Waves Random Complex Media* 1–24.
- Ogawa, S., Kimata, M.: Metal-insulator-metal-based plasmonic metamaterial absorbers at visible and infrared wavelengths: a review. *Materials* **11**, 458 (2018)
- Patel, S.K., Parmar, J.: Highly sensitive and tunable refractive index biosensor based on phase change material. *Phys. B Condens. Matter.* **622**, 413357 (2021)
- Patel, S.K., Charola, S., Jani, C., Ladumor, M., Parmar, J., Guo, T.: Graphene-based highly efficient and broadband solar absorber. *Opt. Mater. (amst)* **96**, 109330 (2019)
- Patel, S.K., Parmar, J., Kosta, Y.P., et al.: Design of graphene metasurface based sensitive infrared biosensor. *Sens. Actuators A Phys.* **301**, 111767 (2020a)
- Patel, S.K., Parmar, J., Katrodiya, D., Nguyen, T.K., Holdengreber, E., Dhasarathan, V.: Broadband metamaterial-based near-infrared absorber using an array of uniformly placed gold resonators. *J. Opt. Soc. Am. B* **37**, 2163–2170 (2020b)
- Patel, S., Parmar, J., Katrodiya, D., Nguyen, T.K., Holdengreber, E., Vigneswaran, D.: broadband metamaterial-based near-infrared absorber using array of uniformly placed gold resonators. *J. Opt. Soc. Am. B* **37**(7), 2163–2170 (2020c)
- Patel, S.K., Charola, S., Parmar, J., Ladumor, M., Ngo, Q.M., Dhasarathan, V.: Broadband and efficient graphene solar absorber using periodical array of C-shaped metasurface. *Opt. Quantum Electron.* **52**(5), 1–19 (2020d)
- Patel, S.K., Surve, J., Parmar, J., Nguyen, T.K.: Review on graphene-based absorbers for infrared to ultraviolet frequencies. *J. Adv. Eng. Comput.* **5**, 214–238 (2021a)
- Patel, S.K., Parmar, J., Zakaria, R.B., Sharafali, A., Nguyen, T.K., Dhasarathan, V.: Sensitivity analysis of metasurface array-based refractive index biosensors. *IEEE Sens. J.* **21**, 1470–1477 (2021b)
- Patel, S.K., Parmar, J., Katkar, V.: Graphene-based multilayer metasurface solar absorber with parameter optimization and behavior prediction using long short-term memory model. *Renew Energy* **191**, 47–58 (2022a)
- Patel, S.K., Surve, J., Jadeja, R., Katkar, V., Parmar, J., Ahmed, K.: Ultra-wideband, polarization-independent, wide-angle multilayer swastika-shaped metamaterial solar energy absorber with absorption prediction using machine learning. *Adv. Theory Simul.* **2022**, 2100604 (2022b)
- Patel, S.K., Parmar, J., Katkar, V.: Metasurface-based solar absorber with absorption prediction using machine learning. *Opt. Mater. (amst.)* **124**, 112049 (2022c)
- Rufangura, P., Sabah, C.: Graphene-based wideband metamaterial absorber for solar cells application. *J. Nanophotonics* **11**(3), 036008 (2017)
- Sang, T., Gao, J., Yin, X., Qi, H., Wang, L., Jiao, H.: Angle-insensitive broadband absorption enhancement of graphene using a multi-grooved metasurface. *Nanoscale Res. Lett.* **14**, 1–8 (2019)
- Saurabh, Y.K., Jha, P.A., Dubey, P.K., Jha, P.K., Singh, P.: Bandgap engineering in TiO₂/rGO 1D photonic metasurfaces as broadband solar absorber. *J. Appl. Phys.* **131**, 023106 (2022)
- Sekhi, S.Z., Shokooh-Saremi, M., Mirsalehi, M.M.: Ultra-broadband, wide-angle, and polarization-insensitive metamaterial perfect absorber for solar energy harvesting. *J. Nanophotonics* **14**(04), 040614 (2020)
- Shen, Q., Xiong, H.: An amplitude and frequency tunable terahertz absorber. *Results Phys.* **34**, 105263 (2022)
- Smith, D.R., Vier, D.C., Kroll, N., Schultz, S.: Direct calculation of permeability and permittivity for a left-handed metamaterial. *Appl. Phys. Lett.* **77**, 2246–2248 (2000)
- Surve, J., Parmar, J., Patel, S.K., Jadeja, R.: Comparative analysis of metasurface array-based solar absorber for visible region. *Opt. Quantum Electron.* **53**(12), 696 (2021)

- Te, L.K., Lin, H., Yang, T., Jia, B.: Structured graphene metamaterial selective absorbers for high efficiency and omnidirectional solar thermal energy conversion. *Nat. Commun.* **11**(1), 1–10 (2020)
- Vafapour, Z., Ghahraloud, H., Keshavarz, A., et al.: The potential of Refractive Index nanobiosensing using a multi-band optically tuned perfect light metamaterial absorber. *IEEE Sens. J.* **21**, 13786–13793 (2021)
- Veselago, V.G.: The electrodynamics of substances with simultaneously negative values of permittivity and permeability. *Sov. Phys. Uspekhi* **10**, 504–508 (1968)
- Wan, C., Chen, L., Cryan, M.J.: Broadband metasurface absorber for solar thermal applications. *J. Opt.* **17**(12), 125103 (2015)
- Yu, P., Chen, X., Yi, Z., et al.: A numerical research of wideband solar absorber based on refractory metal from visible to near infrared. *Opt. Mater. (amst.)* **97**, 109400 (2019)
- Zhang, H., Luo, M., Zhou, Y., Ji, Y., Chen, L.: Ultra-broadband, polarization-independent, wide-angle near-perfect absorber incorporating a one-dimensional meta-surface with refractory materials from UV to the near-infrared region. *Opt. Mater. Express* **10**, 484–491 (2020)

Publisher's Note Springer Nature remains neutral with regard to jurisdictional claims in published maps and institutional affiliations.

Springer Nature or its licensor (e.g. a society or other partner) holds exclusive rights to this article under a publishing agreement with the author(s) or other rightsholder(s); author self-archiving of the accepted manuscript version of this article is solely governed by the terms of such publishing agreement and applicable law.